ChemPlusChem

Research Article
doi.org/10.1002/cplu.202300413

Chemistry Europe
European Chemical Societies Publishing

www.chempluschem.org

Special Collection

Impact of Porous Silica Nanosphere Architectures on the Catalytic Performance of Supported Sulphonic Acid Sites for Fructose Dehydration to 5-Hydroxymethylfurfural

Cameron-Alexander H. Price[+, a, b, c] Antonio Torres-Lopez[+, a, b, c] Robert Evans,[d] Nicole S. Hondow,[e] Mark A. Isaacs,[f, g] Aina Syahida Jamal,[a, b, c] and Christopher M. A. Parlett*[a, b, c, h]

5-hydroxymethylfurfural represents a key chemical in the drive towards a sustainable circular economy within the chemical industry. The final step in 5-hydroxymethylfurfural production is the acid catalysed dehydration of fructose, for which supported organoacids are excellent potential catalyst candidates. Here we report a range of solid acid catalysis based on sulphonic acid grafted onto different porous silica nanosphere architectures, as confirmed by TEM, N_2 porosimetry, XPS and ATR-IR. All four catalysts display enhanced active site normalised activity and productivity, relative to alternative silica supported equivalent systems in the literature, with in-pore diffusion of both substrate and product key to both performance and humin formation pathway. An increase in-pore diffusion coefficient of 5-hydroxymethylfurfural within wormlike and stellate structures results in optimal productivity. In contrast, poor diffusion within a raspberry-like morphology decreases rates of 5-hydroxymethylfurfural production and increases its consumption within humin formation.

Introduction

The transition from the current linear economy within the chemical industry to a circular one requires the development and expansion of catalyst systems with the capacity to process new sustainable feedstocks, of which biomass is anticipated to be a key player.[1] Non-edible lignocellulose represents an ideal feed for the chemical industry given its abundance in nature and within waste streams, the capacity for conversion into a wide array of chemicals and fuels, which are either direct replacements or potential substitutes to current key chemical species, and the elimination of the *food vs fuel* dilemma.[2] 5-hydroxymethylfurfural (5-HMF) is one key platform chemical derived from cellulose via saccharification and subsequent glucose isomerisation to fructose (shown in Scheme 1).[3] The last step is the Brønsted acid catalysed dehydration of fructose to 5-HMF.[4] However, this final step within the overall biomass valorisation process is hindered by further unwanted side reactions which yield undesirable by-products, including humins, i.e. low-value polymeric species. The formation of these proceeds through 5-HMF hydration to 2,5-dioxo-6-hydroxyhexanal, which further undergoes condensation reactions, i.e. aldol reaction, with 5-HMF or fructose (and glucose).[5] This is exacerbated by the presence of the catalysts and high reaction temperatures.[6] Developing catalytic systems that can operate with reduced catalyst loading and reaction temperatures while

[a] *Dr. C.-A. H. Price,[+] A. Torres-Lopez,[+] A. S. Jamal, Dr. C. M. A. Parlett*
Department of Chemical Engineering
The University of Manchester
Manchester, M13 9PL (UK)
E-mail: christopher.parlett@manchester.ac.uk

[b] *Dr. C.-A. H. Price,[+] A. Torres-Lopez,[+] A. S. Jamal, Dr. C. M. A. Parlett*
UK Catalysis Hub
Research Complex at Harwell
Rutherford Appleton Laboratory
Oxfordshire, OX11 0FA (UK)

[c] *Dr. C.-A. H. Price,[+] A. Torres-Lopez,[+] A. S. Jamal, Dr. C. M. A. Parlett*
University of Manchester at Harwell
Oxfordshire, OX11 0DE, UK

[d] *Dr. R. Evans*
Aston Institute of Materials Research
Aston University
Birmingham, B4 7ET (UK)

[e] *Dr. N. S. Hondow*
School of Chemical and Process Engineering
University of Leeds
Leeds LS2 9JT (UK)

[f] *Dr. M. A. Isaacs*
HarwellXPS
Research Complex at Harwell
Rutherford Appleton Lab
Didcot OX11 0FA (UK)

[g] *Dr. M. A. Isaacs*
Department of Chemistry
University College London
London WC1H 0AJ (UK)

[h] *Dr. C. M. A. Parlett*
Diamond Light Source
Harwell Science and Innovation Campus
Oxfordshire, OX11 0DE (UK)

[+] *These authors contributed equally to this work.*

Supporting information for this article is available on the WWW under https://doi.org/10.1002/cplu.202300413

Part of a Special Collection on Green Chemistry

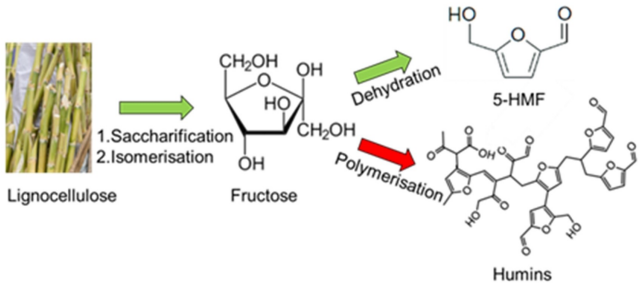

Scheme 1. 5-HMF production from lignocellulosic biomass.

still maintaining high activities is therefore paramount to attempts to drive down unwanted humins and optimise 5-HMF yields.

Supported sulphonic acids have been widely explored for the production of 5-HMF from fructose dehydration, often with a preference for conducting such studies in dimethyl sulphoxide (DMSO). However, DMSO is known to provide high background rates of fructose dehydration to 5-HMF without the addition of the catalyst,[6b] and given its high boiling point, it is far from ideal from an industrial perspective due to increased energy demands of product isolation and purification.[3b,7] In comparison, water scores highly for both green credentials and safety,[8] while also decreasing background rates towards fructose dehydration.[9] Moreover, water can be coupled within biphasic reaction systems, enabling the extraction of reactively formed products into a second organic phase.[6b,10] Sulphonic acids have been incorporated within high surface area supports, including SBA-15,[11] SBA-16,[12] KIT-6,[13] and SAPO-34,[14] and deployed in fructose dehydration. While conversions are often high,[11a,14] reaction conditions are often favourable, comprising low substrate to active site mol ratios. However, yields in most cases are low due to high levels of humins and by-products, while normalised activities/turnover frequencies are poor. Swapping to DMSO can typically impart at least a doubling of 5-HMF yields,[11a,12b, 14] although as background rates for the two solvents are not reported, the precise origin of this is unclear, i.e. catalyst, solvent, or a combination of both. Alternatively, adding an immiscible organic phase, for example, methyl isobutyl ketone (MIBK) and 2-butanol or nitromethane,[15] can achieve similar enhancements through the prevention of subsequent reactions of 5-HMF via its extraction into the organic phase.

High surface area porous silicas are important materials central to various technologies, including catalysis,[16] where their inherent properties make them of interest as support materials. Due to their tuneable physical properties, including surface areas up to ~1000 $m^2 g^{-1}$ and pore diameters, spanning micro, meso, and macropore domains, they have found widespread interest, in particular since the first reports of ordered mesoporous silicas in the 90s, such as MCM-41, SBA-15, and KIT-6.[17] These families of silicas are some of the most studied mesoporous oxides, with synthetic routes developed to tune morphology,[18] chemical composition, including incorporating heteroatoms and organic functionality,[19] control over complementary microporosity,[20] and the introduction of secondary porosity, e.g. macroporosity, to produce hierarchical porous architectures,.[21] Moreover, synthesis under flow conditions provides approaches for their continuous production.[22]

Porous silica nanospheres represent an alternative collection of mesoporous silicas. Mesoporous silicas nanospheres have been produced with a range of different mesopore architectures, including ordered hexagonal arrays of cylindrical pores, similar to those present in MCM-41 and SBA-15,[23] disordered wormlike mesopores,[24] radial cylindrical pores,[25] and other configurations which have typically been named based on their structures, with systems including stellate,[24a,26] wrinkled,[27] and raspberry.[24a] In the case of radial, wrinkled, and stellate architectures, pores, either cylindrical or slit-like, radiate from the centre of the nanosphere, whereas wormlike and raspberry are random arrangements of cylindrical and spherical pores. For MCM-41 and SBA-15 nanospheres, the ordered pore networks arrange in *P6 mm* symmetry, in either a radial fashion from the centre or parallel to each across the diameter of the sphere.[23] Radial, stellate and wrinkled are typically observed for spherical or spherical-like particle morphologies, while ordered hexagonal arrays of cylindrical pores and disordered wormlike mesopores are common within a range of particle morphologies. Despite the chemical and structural features shared with mesoporous silicas, silica nanospheres have typically been less explored as potential catalyst support structures.

Here we report the deployment of mesoporous silica nanospheres with different pore architectures, namely, wormlike, radial, stellate and raspberry, as support architectures for sulphonic acids, via aqueous grafting of 3-mercaptopropyl triethoxysilane and subsequent oxidation of the thiol functional group. The resulting catalysts have been deployed for aqueous fructose dehydration at relatively low temperatures and benchmarked against alternative silica sulphonic acid catalysts. Given the equivalent nature of the catalysts, i.e. sulphonic acids on silicas, any differences in active site normalised activities (i.e. turnover frequencies) will arise only due to differences in in-pore mass transfer. To explore this, pulsed-field gradient Nuclear Magnetic Resonance (PFG-NMR)[28] measurements of the in-pore diffusion coefficients of reagents and products will be used, an approach that is gaining traction within the field.[29]

Results and Discussion

Silica nanosphere characterisation

The different pore architectures of the four classes of silica nanospheres, radial, stellate, wormlike and raspberry, are confirmed through a combination of nitrogen porosimetry and TEM. Isotherms and electron micrographs are consistent with the literature,[24a,25a] with surface areas and average pore diameters reported in Table 1 and isotherms, pore size distributions and micrographs shown in Figures 1, S1, and S2. TEM reveals the unique mesopore architectures of the supports, in which wormlike possess disordered cylindrical pores, stellate presented channel like mesopores, radial comprises cylindrical

Table 1. Textural properties of the silica nanosphere supports.

Support	BET/ $m^2 g^{-1}$	Micropore SA[a]/$m^2 g^{-1}$	NLDFT (BJH)[b]/nm	Ave. particle size/nm
Wormlike	801 ± 80	219 ± 22	3.5 (2.9)	104 ± 12
Stellate	468 ± 47	99 ± 10	30.5 (17.5)	108 ± 15
Radial	347 ± 35	61 ± 6	8.4 (5.4)	97 ± 8
Raspberry	564 ± 56	223 ± 22	3.1 (2.0)	39 ± 4

[a] SA = surface area [b] Pore diameter with BJH in parenthesis.

pores that radiate the sphere centre, while raspberry displays spherical mesopore.[24a,25a] BJH pore sizes allow comparison with the original publications. However, as these are known to underestimate pore sizes, NLDFT values are reported.[30] The wormlike nanospheres exhibit a typical type 4 isotherm, without hysteresis, consistent with the presence of small mesopores (average size of 3.5 nm by NLDFT). These nanospheres possess the highest surface area (both total and mesopore surface area) of the four supports. Radial and raspberry nanospheres also show type 4 isotherms, resulting from the small intraparticle mesopores and a high proportion of large interparticle voids. In contrast, the stellate silica spheres present a type 2 isotherm,

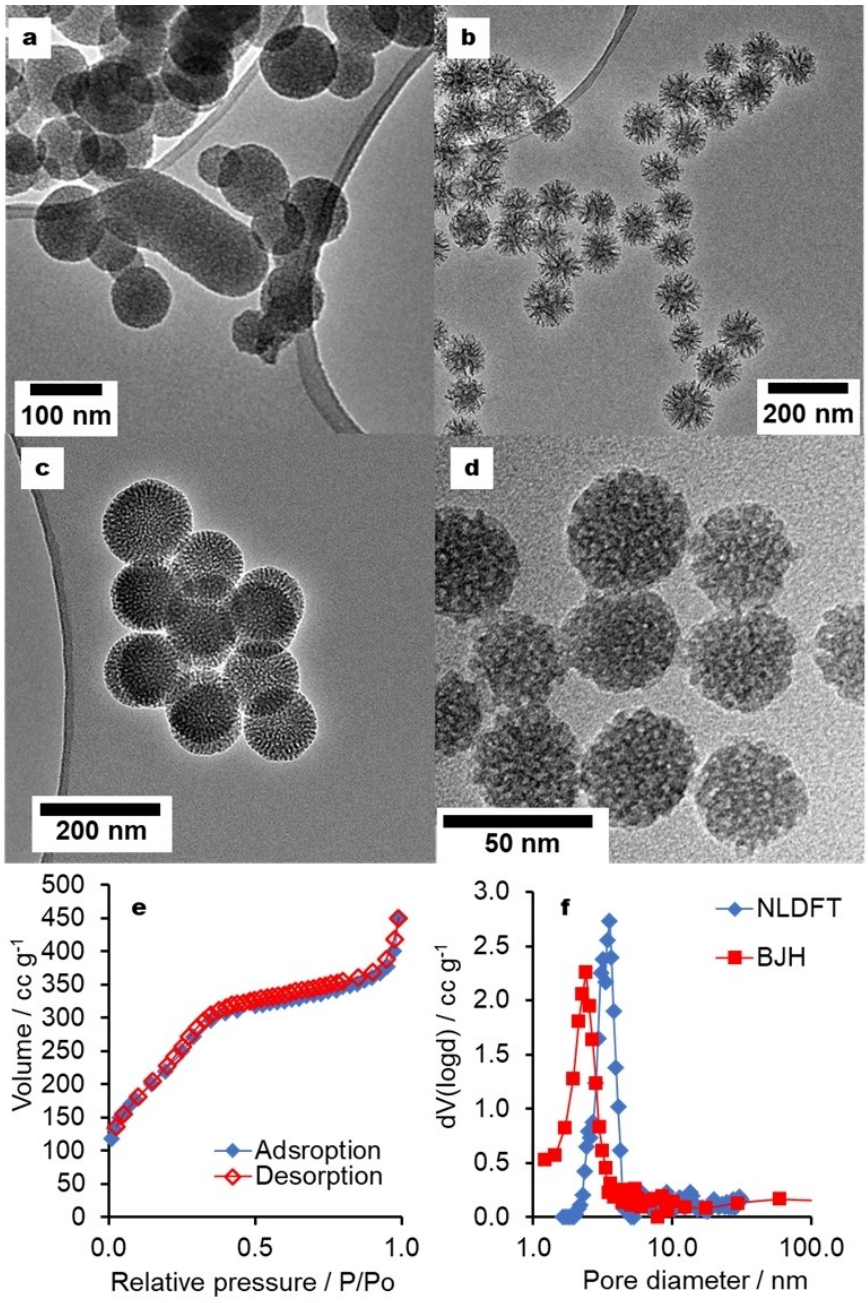

Figure 1. High magnification electron micrographs of (a) wormlike, (b) stellate, (c) radial, and (d) raspberry silica nanosphere supports, and (e) nitrogen adsorption isotherms and (f) pore size distribution for wormlike silica nanosphere support.

reflecting the larger mesopores and macropores. TEM images confirm the assignment of intraparticle mesopores, revealed by the N_2 isotherms and pore size distribution plots. Wormlike, stellate and radial show comparable average particle sizes, in the region of 100 nm, whereas the raspberry morphology support is approximately half the diameter.

Acid catalyst characterisation

Aqueous grafting of sulphonic acid functional groups, through covalently linking of 3-mercaptopropyl trimethoxy silane and subsequent thiol oxidation, is shown to have no significant impact on silica nanosphere particle size (Figures 2 and S3), while EDX mapping confirms uniform dispersion of sulphur across the porous architecture of the support (Figure S4). Moreover, acid site incorporation shows only a minor impact on the textural properties evaluated by nitrogen porosimetry (Figure 2 and S5), consistent with surface grafting of organosilanes.[21a,31] Preservation of the parent isotherm shape is apparent, albeit with reduced amounts of N_2 adsorbed, indicating a decrease in both surface area and mesopore diameter size (Table 2).[32] The latter being consistent with the deposition of the organic functional group (RSO_3H) within the mesopores of all four different silica nanosphere morphologies.

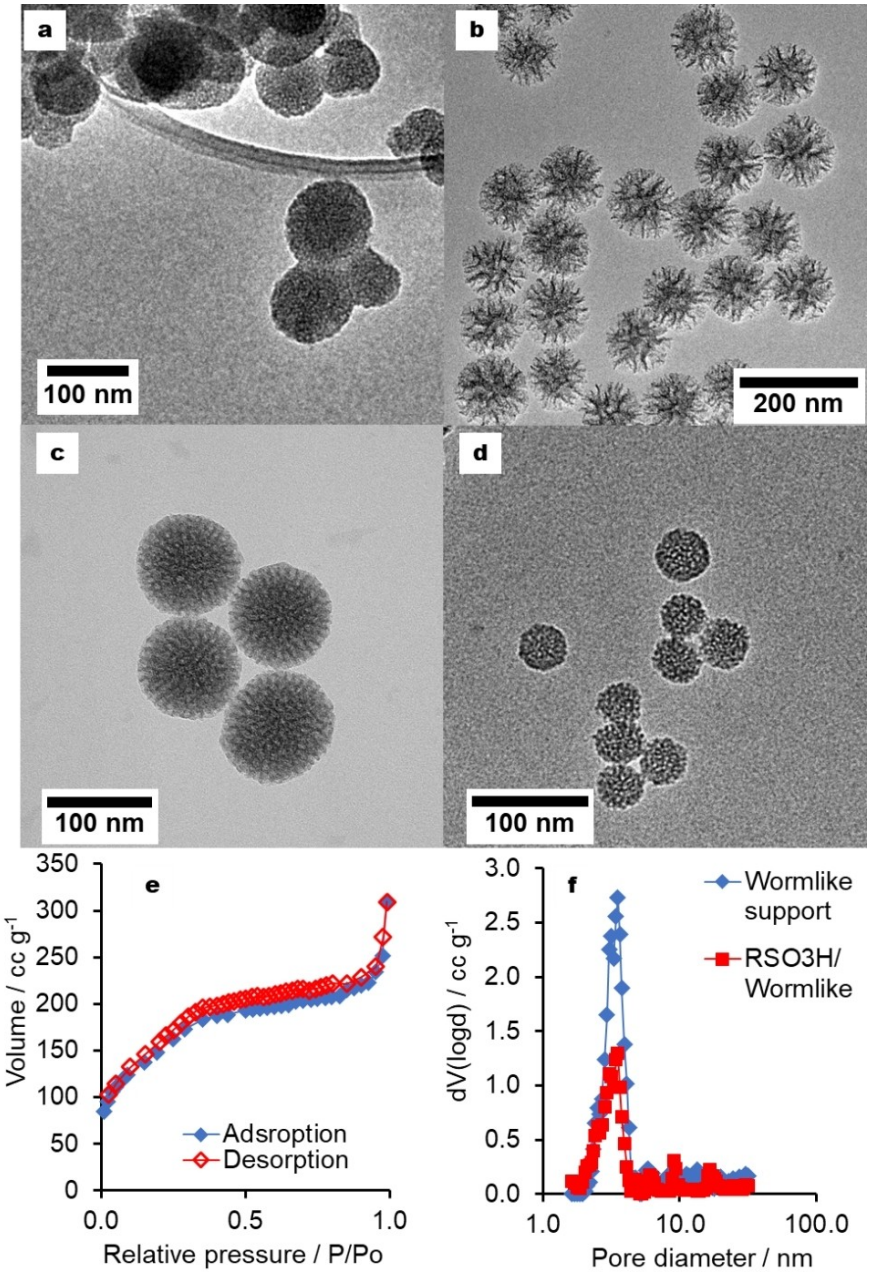

Figure 2. High magnification electron micrographs of (a) RSO_3H/wormlike, (b) RSO_3H/stellate, (c) RSO_3H/radial, and (d) RSO_3H/raspberry silica nanosphere catalysts, and (e) nitrogen adsorption isotherms and (f) NLDFT pore size distribution for wormlike silica nanosphere support and RSO_3H/wormlike catalyst.

Table 2. Textural properties of the silica nanosphere acid catalysts.

Support	BET/ $m^2 g^{-1}$	Micropore SA[a]/m^2 g^{-1}	NLDFT (BJH)[b]/nm	Acid[c]/ mmol g^{-1}
RSO^3H/ Wormlike	538 ± 54	250 ± 25	3.4 (2.4)	0.57
RSO^3H/ Stellate	283 ± 28	0	28.4 (29.4)	0.66
RSO^3H/Radial	272 ± 27	0	7.9 (4.3)	0.37
RSO^3H/ Raspberry	313 ± 31	89 ± 9	2.5 (2.1)	0.54

[a] SA = surface area [b] Pore diameter with BJH in parenthesis [c] Acid site loading from pulse titration NH_3 chemisorption.

Attenuated total reflection-infrared spectroscopy was deployed to further confirm the deposition of 3-mercaptopropyl trimethoxysilane and its oxidation to grafted sulphonic acids. As shown in Figures 3 and S6, SH stretching at 2557 cm^{-1} from the thiol is detected for all four materials,[33] with the species fully consumed upon oxidation with H_2O_2. Further evidence of successful grafting is apparent in the CH stretching region. However, due to the hydrophilic nature of the acid catalysts,[34] the OH region partially obscures these features, particularly for the sulphonic acid variants. Confirmation of the presence of sulphonic groups by IR is prohibited due to the S=O stretching region overlapping by the Si–O bands, which are the dominant species given the composition of the catalytic materials.[35] X-ray photoelectron spectroscopy (XPS) was thus deployed to confirm the presence of sulphonic acid groups, as shown in Figure 3d, with the S2p binding energy increasing from ~164 to ~169 eV, consistent with the existing literature values.[21a,32] Sulphur loadings from XPS spanned from 3.1 at.% to 1.7 at.%, consistent with the previous literature for aqueous grafting of sulphonic acid.[32] Acid site loadings were evaluated by NH_3 pulse titrations and are reported in Table 2. Values in the region of ~0.6 mmol g^{-1} align with the value of 1.4 mmol g^{-1} previously reported for SBA-15, a mesoporous silica with a surface area in the region of 800 $m^2 g^{-1}$.[36]

PFG-NMR was deployed to assess substrate and product diffusion within the porous catalysts. However, the inhomogeneity from the addition of a solid, magnetic susceptibility differences at the solid-liquid interface, and adsorption interactions combine to give rise to broad, featureless spectra that are difficult to interpret while obtaining precise chemical shifts are impossible. Fortunately, measurements of molecular self-diffusion coefficients are broadly independent of observable chemical shift phenomena, with such measurements depending on the decay of relevant NMR signals as a result of molecular

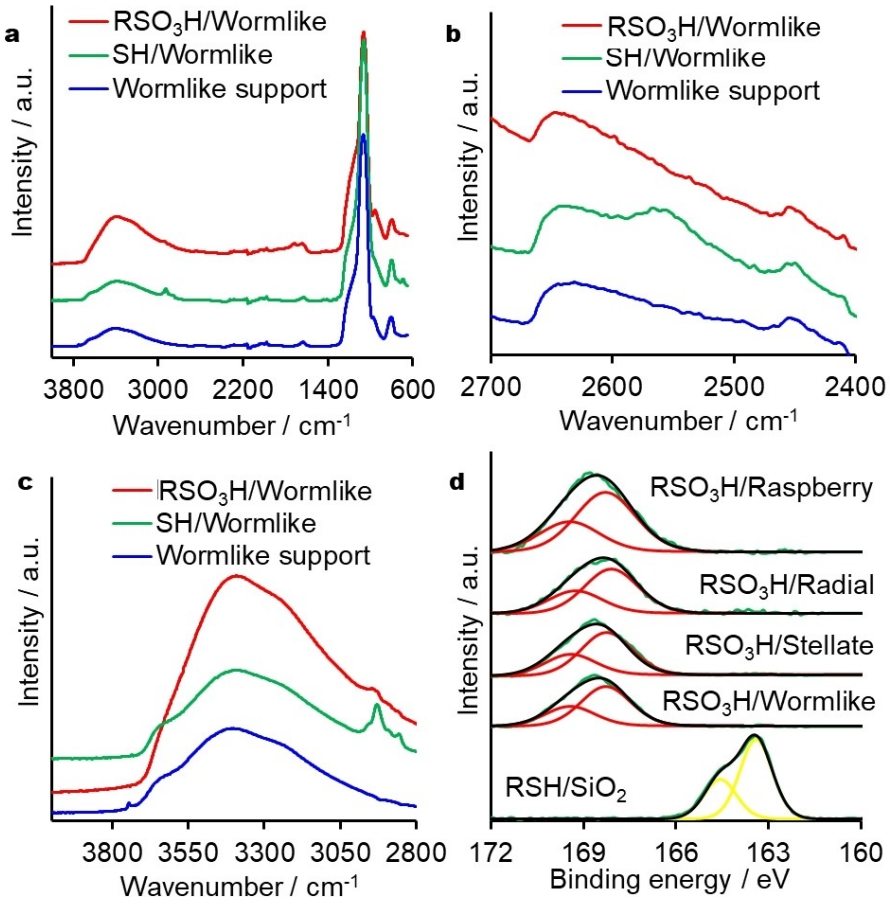

Figure 3. ATR-IR of wormlike support, SH/wormlike catalyst precursor, and RSO_3H/wormlike catalyst (a) full spectra, (b) SH region, (c) CH and OH stretching region, and (d) stacked S2p XPS spectra for the series of RSO_3H catalysts (offset for clarity) and a representative SH/SiO_2 catalyst precursor.

motion.[29c] Thus, PFG-NMR measurements of diffusion provide molecular level information on the different motion of molecules within the differently architectured silica nanospheres. DOSY spectra and Stejskal-Tanner plots are shown in Figures S7–11, with diffusion coefficients of fructose and 5-HMF within the four support materials reported in Figure 4 and Table S1. For both compounds, the in-pore diffusion coefficients for all four supports are reduced relative to their free diffusion in an unconfined bulk aqueous liquid environment, with HMF diffusion coefficients showing a greater decrease relative to fructose. Confinement effects within porous architectures can result in inducing greater diffusion, due to disruption of the localised hydrogen bonding network,[29b] the same is not apparent here, possibly as the effect is substrate and support dependent.[29a] However, this disruption may be the factor for the lesser impact on fructose diffusion through a partial interference of the intermolecular bonding. Furthermore, it might be intuitive to assume that more open frameworks with larger pore diameters, such as stellate nanospheres, would have faster diffusion through the pores, but this is not the case here. The fastest diffusion was observed through the pores of the wormlike nanospheres.

Catalytic dehydration of fructose

The selective dehydration of fructose to 5-HMF was studied over the four catalysts at 120 °C under autogenous pressure within a Buchi miniclave with agitation, with reaction data shown in Figure 5. Blank reactions, using unfunctionalised silica support, showed negligible conversion after 6 h. In all cases, after the initial 30 minutes of the reaction, it becomes apparent that there is a degree of catalyst deactivation, which is more apparent in the formation of 5-HMF (Figures 5a and b). Thus subsequent normalised activities and productivities have been determined over the initial 30 minutes of the catalytic reaction. Turnover Frequencies (TOFs) for both fructose consumption and 5-HMF production are reported in Figure 5c, with values for both outperforming alternative sulphonic acid silicas for aqueous phase fructose dehydration (discussed in detail later). Given that the only variable in the four catalysts is pore architecture, i.e. they all comprise of the same material with an identical nature of the acid sites present, and that TOFs are normalised to acid site loadings, the question arises as to whether the order of catalyst activity, for both consumption and formation, correlates with the observed diffusion coefficients from NMR, i.e. in-pore diffusion is the governing factor. As stated above, larger pores do not necessarily result in greater in-pore diffusion, as shown by the results for stellate framework relative to wormlike. Figures 5d and S12 clearly show that both the conversion of fructose and the production of 5-HMF display a linear correlation to the molecule's diffusion coefficients within the four support architectures. Thus, for catalyst systems in which all active sites are equal in chemical nature and are quantifiable so that differences in loading can be factored, as would be logically expected, diffusion coefficients of the species constrained within the porous support matrix represent an excellent descriptor of catalyst performance.

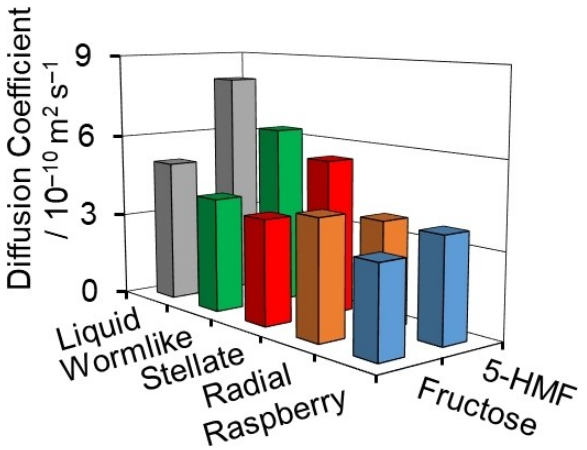

Figure 4. PFG-NMR acquired diffusion coefficients for the substrate (fructose) and product (5-HMF) in bulk liquid and within the four catalysts.

Increasing the reaction length beyond the initial 30 minutes reveals the onset of a decrease in the process mass balances, which coincides with the reaction solution colour changing from clear to yellow and then brown. This is due to the formation of humins, the undesirable polyfuranic by-product that plagues acid catalysed saccharide dehydration reactions.[3a] It is reported that 5-HMF is converted to 2,5-dioxo-6-hydroxyhexanal, via subsequent hydration,[37] which rapidly reacts via acid catalysed aldol condensations with aldehydes and ketones present,[5a] namely 5-HMF or fructose.[5b] This being catalysed by the presence of the solid Brønsted acid mesoporous silicas. The missing mass balance here, i.e. material not analysed by HPLC and removed prior to by filtration, is attributed to these insoluble humins. No other products were detected by HPLC, including levulinic acid and formic acid,[38] produced by subsequent hydration and dehydration and carbon bond cleavage, which results via an acid catalysed cascade process in which 5-HMF is an intermediate.[39] This is typically reported at higher temperatures than this study, often for longer reactions and employing strong liquid Brønsted acids, such as H_2SO_4 or HCl.[40]

In the case of the stellate support, humins are the dominant species after 6 hours (end of the reaction), with this greater degree of humin formation over the largest pore system consistent with the report of increases in humin formation for sulphonic acid functionalised large pore SBA-15 relative to smaller pore equivalents, BJH pore sizes of ~14 vs 4 nm, due to greater accessibility of the acid active sites.[41] This, combined with the greatest fructose conversion over the stellate catalyst, suggest that the open framework with the large pore diameter retains a greater degree of acid site accessibility even in the face of considerable humin levels. In contrast to the stellate system, in which 2,5-dioxo-6-hydroxyhexanal is reacting with both fructose and 5-HMF, the raspberry system has a relative preference for humin formation to occur via the reaction of 2,5-dioxo-6-hydroxyhexanal with 5-HMF, as evidenced by the drop in 5-HMF yield after 1.5 h. Thus the reaction of 5-HMF formation from fructose dehydration is slower than that of 5-HMF

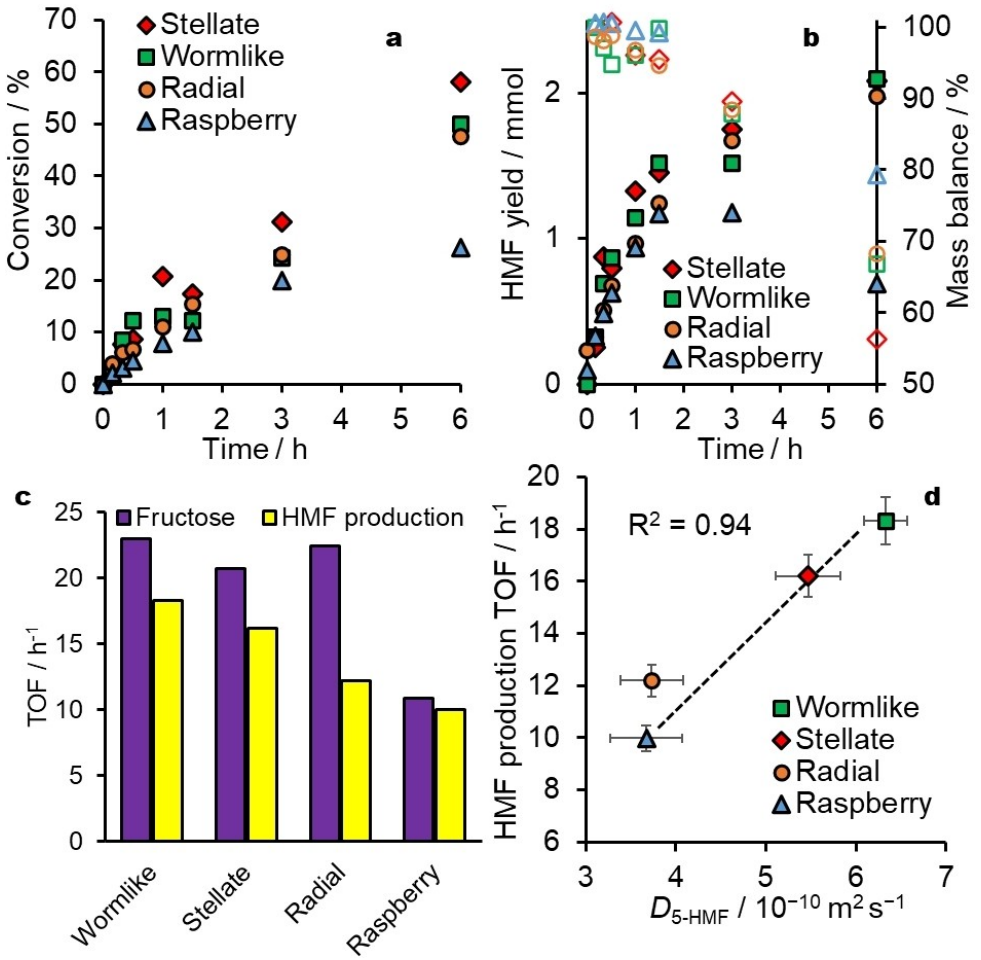

Figure 5. Catalytic performance data for fructose dehydration to 5-HMF at 120 C, showing (a) fructose conversion reaction profiles, (b) 5-HMF yield profiles and reaction mass balances, (c) fructose consumption and 5-HMF production TOFs calculated using rate over the initial 0.5 h and NH_3 chemisorption acid site loadings, and (d) correlation between 5-HMF production TOFs and 5-HMF diffusion coefficients within the silica support structures.

consumption through humin formation. This is only observed for the RSO_3H/raspberry system and is attributed to a greater overall drop in fructose and 5-HMF diffusion coefficients of the confined species relative to unrestricted values. This reduced diffusion of 5-HMF and fructose increases the potential for unwanted reactions with 2,5-dioxo-6-hydroxyhexanal, due to their extended residence within the pores. As with the RSO_3H/stellate, the catalyst system based on radial and wormlike supports show only a slowing in the yield of 5-HMF, which continues to slow with time. Thus for these systems, the production of humins does not show a preference towards 2,5-dioxo-6-hydroxyhexanal reacting with 5-HMF. This arises due to either greater 5-HMF diffusion coefficients, reduced residence within the pore, or greater fructose diffusion, i.e. increased diffusion of fructose into the architecture and increased chance of encountering it.

A comparison of the four catalysts reported here is made to other sulphonic acid catalysts under comparable conditions. Water has been chosen as an ideal green solvent to avoid the unwanted contributions from DMSO,[6b] so that a clearer picture of the inherent activity of the different catalyst systems can be obtained. Comparisons have focused on systems in which sulphonic acid sites are supported predominantly on silica support frameworks, given the relative inertness and inherent lack of strong acidity, i.e. compared to alumina silicates.[42] Ideally, comparisons would be made through turnover frequencies,[43] both for fructose consumption and 5-HMF production, preferably at 120 °C or temperatures close to. However, many studies are conducted with only a slight excess of fructose relative to the number of acid sites deployed. Such conditions also result in favourable conversions and yields, so comparing these is not straightforward either. Catalyst performances are reported in Table S2, with the silica nanosphere systems performing favourably when evaluated through 5-HMF production TOFs.

Sulphonic acid catalysts based on the ubiquitous mesoporous silica, SBA-15, have been reported by Wang et al. and Whitaker and co-workers,[11] with both employing almost identical approaches to catalyst synthesis and both deploying their catalyst at 120 °C. Thus it might be intuitive to assume similar performances would be reported. However, this is not the case. Due to significantly different substrate:active site mol

ratios, 3 vs 50, conversion and 5-HMF yields are reported to reach 100% and 58% after 1 h in contrast to only 44% and 15.4% over 48 hours. Another of the SBA family, namely SBA-16, has also been functionalised via the same synthesis protocol, with this achieving a 5-HMF yield of 26% (substrate: active site mol ratio 20) at 110 °C,[12a] while KIT-6, another mesoporous silica support, produced via co-condensation of the acid precursor and the support, achieved a yield of 3% (substrate:active site mol ratio 26) for a reaction temperature of 135 °C.[13] Comparisons of TOFs based on 5-HMF production reveals SBA-16 to be the most active, with a TOF of 3.6 h^{-1}, potentially due to greater in-pore diffusion through the 3-dimensional mesopore network, followed by KIT-6, 1.2 h^{-1}, and then SBA-15 0.9 h^{-1} (Wang) and 0.2 h^{-1} (Whitaker). Sulphonic acids have likewise been grafted on SAPO-34, with reaction in water at 160 °C and with a substrate:active site mol ratio of 15 yielding 5-HMF production TOFs of 1.6 h^{-1}, with conversion reaching 80% in 45 minutes although with a yield of only 8%.[14] The higher reaction temperature and inherent acidity of SAPO-34[44] would be expected to increase TOFs, although the smaller micropores of SAPO-34 and the resulting mass diffusion limitation are likely the controlling parameter. Core-shell systems have also been reported, with Fe_3O_4@SiO_2-SO3H providing a magnetically separable catalysts with a 5-HMF production TOF of 1.4 h^{-1} at 120 °C and a mol ratio of 15.[10] Fructose conversion and 5-HMF yields of 73.4% and 14.2%, respectively, were obtained after 1.5 h.

Further advances to improve process selectivity in the production of 5-HMF in aqueous phase systems have focused on deploying biphasic systems, in which an organic phase is added to extract the 5-HMF as it is produced to prohibit its further conversion. The addition of a mixture of MIBK and 2-butanol is a commonly reported extraction phase employed. It is shown to increase 5-HMF production TOFs for sulphonic acid grafted SBA-15, akin to those discussed above, to 11.4 h^{-1} at 130 C,[15a] while at 160 °C it increases to 490 h^{-1},[15b] for comparable substrate:active site mol ratios of ~40. Further catalyst development, including modifying the grafted organo-acid or using periodic mesoporous organosilica SBA-15, can further tune catalyst performance.[15a,b] Nitromethane is another extraction phase that has been employed in conjunction with sulphonic acid grafted SAB-15. At 130 °C, a 5-HMF production TOF of 36 h^{-1} is calculated over the initial 0.5 h.[15c] An increase in reaction temp to 140 °C induces a 30% increase, however, coupling this increase with co-grafting benzyl functional group to increase results in only a 6% increase. An alternative approach to enhance process selectivity, through the minimisation of humin formation, is to convert the reactive formed 5-HMF into a more stable product before can undergo conversion into humins. The coupling of a magnetic-core-acid-shell dehydration catalyst (Fe_2O_3@SiO_2-SO_3H) with an oxidation catalyst ($ZnFeRuO_4$) result in the production 2,5-diformylfuran, with high yields (90%) albeit in DMSO, via a one-pot two-step cascade process enabled through changing the gas composition after the first step. The first step of the cascade, the acid catalysed dehydration, can proceed in water although yields are modest at 14.2% compared to 96.1% in DMSO, with conversions of 73.4% and 100%, respectively.[10]

Characterisation of the spent catalysts was conducted to investigate potential poisoning via deposition of humins. ATR-IR and XPS (Figures S13 and S14) reveal significant C deposition on the spent catalysts. CH stretching bands at 2940 cm^{-1} wavenumbers, consistent with alkane stretches and features at 1630 and 1525 cm^{-1} wavenumbers, can be attributed to carbonyl groups conjugated with carbon-carbon double bonds and the furan ring, respectively. While the peaks spanning 1300–1475 cm^{-1} wavenumbers are consistent with humins from fructose.[5] XPS further confirms the presence of significant C–O species via deconvolution, the being dominant C species present and corresponding to alcohol and ether functional groups. Furthermore, significant levels of C at higher binding energy are also apparent, which can be attributed to carboxylate and ester functional groups. Both are consistent with the oxygenated poly-furanic structure of humins. C content of the spent wormlike and raspberry catalysts are 17 and 21 at.% respectively. Thus, the raspberry structure appears to be more heavily affected by humin deposition. While this does result in a drop in apparent S loadings to only 0.6 and 0.3 at.% accordingly, due to the increased C content, no apparent shift in the S binding energy is witnessed, thus, it would appear they are retained in the sulphonic acid state. Developing a facile route to remove this carbon is, therefore, critical to producing a fully recyclable catalyst.

Conclusions

Mesoporous silica nanospheres represent exciting frameworks for catalysts, with functionalisation through grafting of organosilane sulphonic acids introducing catalytic activity for fructose dehydration to 5-HMF, a bioderived platform chemical critical to the future of biorefinery concept. Through fine-tuning the nanosphere pore architecture, it is shown that enhancement in catalytic performance can be realised. Structure-activity correlations, through evaluating PFG-NMR derived diffusion coefficients and TOFs, it is clear that diffusion of both substrate and product within the porous material is the governing factor on overall process performance. TOFs exceeding 20 h^{-1} for fructose conversion and 15 h^{-1} for 5-HMF production represent significant enhancements on the existing literature for silica support sulphonic acids under comparable reaction conditions. Furthermore, it is reasonable that such systems would benefit through their deployment within biphasic reaction systems or one-pot cascade reactions.

Experimental

Support synthesis: Dendritic radial mesoporous silica nanospheres were synthesised using the biphasic approach reported by Shen et al.[25a] Cetyltrimethylammonium chloride (25% v/v in water, 240 cm^3), triethanolamine (TEA, 1.8 g), and water (360 cm^3) were stirred at 120 rpm for 1 h at 60 °C. Tetraethyl orthosilicate (40 cm^3) in cyclohexane (160 cm^3) was slowly layered on top of the aqueous

phase to form a biphasic system, which was stirred for 48 h. The solid silica was recovered from the aqueous phase by centrifugation (14500 rpm, 15 min) and washed with water in triplicate before drying at room temperature overnight. The mesopore template was removed by solvent extraction in an ethanolic HCl solution (0.01 M, 100 cm^3 per 1 g of support) under reflux for 24 h, before isolation and calcination at 550 °C for 5.5 h under air (ramp rate 1 °C min^{-1}). Stellate, raspberry, and wormlike silica nanospheres were synthesised using the method of Zhang et al.[24a] For stellate, cetyltrimethylammonium tosylate (9.6 g), triethanolamine (1.735 g), and water (500 cm^3) were agitated at 900 rpm for 1 hour at 80 °C. Tetraethyl orthosilicate (72.9 g) was added quickly and the solution was left for 2 h. The solid was isolated by vacuum filtration and washed in triplicate before drying at room temperature overnight. The mesopore template was removed by calcination at 550 °C for 5.5 h under air (ramp rate 1 °C min^{-1}). Raspberry silica nanospheres were synthesised under the same conditions as stellate with the exception that cetyltrimethylammonium tosylate was replaced by cetyltrimethylammonium bromide and the solid was isolated by centrifugation (14500 rpm, 15 min). Wormlike silica nanospheres were synthesised using cetyltrimethylammonium bromide (1.51 g), triethanolamine (82.88 g) and water (100 cm^3), which were mixed at 900 rpm for 1 h at 80 °C. Tetraethyl orthosilicate (14.47 g) was added quickly and the solution was left for 2 h. Upon completion, the solution was centrifuged (14500 rpm, 15 min) to isolate the solid, which was washed in triplicate and dried at room temperature overnight. The mesopore template was removed by calcination at 550 °C for 5.5 h under air (ramp rate 1 °C min^{-1})

Catalysts synthesis: The silica nanospheres with differing pore architectures were functionalised with sulphonic acid sites.[32] Silica support (2 g) was dispersed in water (60 cm^3) at reflux temperature. 3-mercaptopropyl triethoxysilane (2 cm^3) was added and the solution was refluxed under stirring at 900 rpm for 24 h. The grafted silica was isolated by centrifugation (14500 rpm, 15 min), washed with water in triplicate, and dried overnight at room temperature. The thiol functionalised silicas were converted to the sulphonic acid derivative through oxidation by H_2O_2 (30 wt% 60 cm^3) at room temperature under stirring for 24 h. The catalyst was recovered by centrifugation, washed with water in triplicate, and dried overnight at 80 °C.

Characterisation: Nitrogen porosimetry was conducted using a Quantachrome Quadrasorb porosimeter. Samples were degassed at 150 °C overnight, with N_2 adsorption/desorption isotherms recorded at −196 °C. Surface areas were calculated over the relative pressure ranges 0.02–0.2 and 0.2–0.5 for BET (Brunauer, Emmett and Teller) and t-plot analysis, respectively. Mesopore properties were evaluated using the NLDFT and BJH (Barrett-Joyner-Halenda) methods. For the former, fits to both cylindrical and spherical pores were evaluated with the best fit used, while the latter was applied to the desorption branch of the isotherm. High-resolution (scanning) transmission electron microscopy ((S)TEM) images were recorded on either a JEOL 2100 operating at 200 kV or on an FEI Titan3 Themis G2 operating at 300 kV fitted. The latter was equipped with four energy dispersive X-ray spectrometry (EDX) silicon drift detectors. Samples were prepared by dispersing in methanol and drop-casting onto a holey carbon support film on a copper grid (Agar Scientific). Images were analysed using ImageJ 1.41 software. Attenuated total reflectance infrared spectroscopy (ATR-IR) was performed using a Thermo Nicolet iS 10 Fourier transform infrared spectrometer fitted with a Smart iTR attenuated total reflectance accessory. Spectra were collected as an average of 64 scans with a resolution of 4 cm^{-1}, using air as the background. X-ray photoelectron spectroscopy (XPS) was conducted using a Kratos Axis SUPRA X-ray photoelectron spectrometer fitted with a charge neutraliser and magnetic focusing lens using Al Kα monochromated radiation (1486.7 eV). CasaXPS version 2.3.19 was used for spectra calibration and fitting, with energy referencing to the C 1s peak of adventitious carbon at 284.8 eV. S 2p backgrounds were modelled using a quadratic function of cross-section (4535.29, −17.3355, 2704.68, −9) to account for the rising background from Si 2 s photoelectron energy loss processes and subsequent Shirley-type function. Si $2p^{3/2}$ and $2p^{1/2}$ peaks were modelled using a line shape of LA (1.53,243), an energy separation of 1.15 eV, and an area ratio of 2 : 1.PFG-NMR Measurements of Diffusion were carried out, non-spinning, on a 300 MHz Bruker Avance spectrometer, using a 5 mm PABBO BB-1H ZGRD probe equipped with a *z*-gradient coil producing a maximum gradient of 56.4 G cm^{-1}. Each NMR sample contained 20 mM of the substrate, with 2 mM of TSP as a reference, in 85 : 15 mixed CH_3OH-d_4:D2O solution. All NMR measurements were performed at 25 °C and used a double-stimulated-echo bipolar-pulse pair sequence[45] to remove any possible effects of convection from the measurements in bulk solution. The same pulse sequence was then used for all later NMR diffusometry experiments. Ten magnetic field gradient amplitudes, from 32.0 to 3.55 G cm^{-1}, were used and incremented in equal steps of gradient squared. The gradient encoding time for all experiments was 1 ms and all gradients were half-sine in shape. The diffusion delay time, Δ, was set according to the species studied, to obtain *ca.* 80% attenuation of signals. For each gradient amplitude, 32 transients of 16384 complex data points were acquired for a total experimental time of *ca.* 30 min. DOSY spectra and associated diffusion coefficients were subsequently produced using the DOSY Toolbox software package.[46] For catalysts and bulk liquids, 2-dimensional DOSY spectra of fructose and 5-HMF have been produced from the PFG-NMR data. While the presence of the silica broadens all NMR signals, it is possible to obtain estimates of molecular diffusion coefficients, albeit with increased uncertainty. Stejskal-Tanner plots indicating how the diffusion coefficients have been estimated have been produced for indicative fructose and 5-HMF peaks to support the diffusion data further.

Catalyst screening: Fructose dehydration to 5-hydroxymethylfurfural was conducted using a 50 cm^3 glass Buchi minicalve under autogenous pressure. The catalyst (200 mg) and magnetic stirrer were added to an aqueous 5-HMF solution (0.5 M, 20 cm^3), which equates to a substrate:active site mol ratio of ~100 : 1, and added into the miniclave, and the system was sealed. The miniclave was heated in an oil bath to the desired reaction temperature (120 °C), with a temperature probe monitoring the reaction solution. Upon reaching the reaction temperature, the reaction was initiated by starting agitation of the system (900 RPM). Reaction aliquots (0.5 cm^3) were collected at regular intervals (0, 10, 20, 30, 60, 90, 180 and 360 minutes) via a dip tube and sampling value, with the catalyst removed by filtration before analysis by HPLC. HPLC analysis was conducted on a Shimadzu UFLC LC-20AD, fitted with a Phenomenex ROA-organic acid column, and Refractive Index and UV detectors. Aqueous 0.005 N H_2SO4 was used as the mobile phase, with a flow rate of 0.5 cm^3 min^{-1} and a column temperature of 40 °C.

Supporting Information

Additional underpinning data is provided in the Electron Supporting Information.

Author Contributions

CAHP: investigation, methodology, formal analysis, visualisation. ATL: investigation, methodology, formal analysis, visualisation. RE: investigation, methodology, formal analysis, visualisation, writing – original draft, funding acquisition. NSH: investigation, visualisation, formal analysis, funding acquisition. MAI: investigation, formal analysis. ASJ: investigation, formal analysis. CMAP: conceptualisation, investigation, methodology, formal analysis, writing – original draft, data curation, supervision, project administration, funding acquisition.

Acknowledgements

CMAP would like to thank the Research Complex for access and support to these facilities and equipment. In addition, the UK Catalysis Hub is kindly thanked for resources and support provided via our membership of the UK Catalysis Hub Consortium and funded by EPSRC grant EP/R027129/1. The X-ray photoelectron (XPS) data collection was performed at the EPSRC National Facility for XPS ("HarwellXPS"), operated by Cardiff University and UCL, under Contract No. PR16195.

Conflict of Interests

The authors declare no conflict of interest.

Data Availability Statement

The data that support the findings of this study are openly available in Figshare at https://doi.org/10.48420/c.6767793, reference number 6767793.

Keywords: diffusion · fructose · 5-hydroxymethylfurfural · nanospheres · sulphonic acid

[1] a) R. A. Sheldon, *J. Mol. Catal. A* **2016**, *422*, 3–12; b) R. Palkovits, I. Delidovich, *Philos. Trans. R. Soc. London Ser. A* **2018**, *376*, 20170064.
[2] a) C. Xu, E. Paone, D. Rodriguez-Padron, R. Luque, F. Mauriello, *Chem. Soc. Rev.* **2020**, *49*, 4273–4306; b) J. Iglesias, I. Martinez-Salazar, P. Maireles-Torres, D. M. Alonso, R. Mariscal, M. L. Granados, *Chem. Soc. Rev.* **2020**, *49*, 5704–5771; c) Y. X. Jing, Y. Guo, Q. N. Xia, X. H. Liu, Y. Q. Wang, *Chem* **2019**, *5*, 2520–2546.
[3] a) J. Slak, B. Pomeroy, A. Kostyniuk, M. Grilc, B. Likozar, *Chem. Eng. J.* **2022**, *429*, 132325; b) R. J. van Putten, J. C. van der Waal, E. de Jong, C. B. Rasrendra, H. J. Heeres, J. G. de Vries, *Chem. Rev.* **2013**, *113*, 1499–1597.
[4] A. Osatiashtiani, A. F. Lee, D. R. Brown, J. A. Melero, G. Morales, K. Wilson, *Catal. Sci. Technol.* **2014**, *4*, 333–342.
[5] a) S. K. R. Patil, C. R. F. Lund, *Energy Fuels* **2011**, *25*, 4745–4755; b) S. K. R. Patil, J. Heltzel, C. R. F. Lund, *Energy Fuels* **2012**, *26*, 5281–5293.
[6] a) J. C. V. Calderon, J. S. Arora, S. H. Mushrif, *ACS Omega* **2022**, *7*, 44786–44795; b) H. Xiang, S. Zainal, H. Jones, X. Ou, C. D'Agostino, J. Esteban, C. Parlett, X. Fan, *RSC Sustain.* **2023**, *1*, 1530–1539.
[7] C. Moreau, M. N. Belgacem, A. Gandini, *Top. Catal.* **2004**, *27*, 11–30.
[8] D. Prat, A. Wells, J. Hayler, H. Sneddon, C. R. McElroy, S. Abou-Shehada, P. J. Dunn, *Green Chem.* **2016**, *18*, 288–296.
[9] S. L. Barbosa, M. D. Freitas, W. T. P. dos Santos, D. L. Nelson, S. I. Klein, G. C. Clososki, F. J. Caires, A. C. M. Baroni, A. P. Wentz, *Sci. Rep.* **2021**, *11*, 1919.
[10] W. Wei, G. Lyu, W. Jiang, Z. Chen, S. Wu, *J. Colloid Interface Sci.* **2021**, *602*, 146–158.
[11] a) L. Wang, L. Zhang, H. Li, Y. Ma, R. Zhang, *Compos. B. Eng.* **2019**, *156*, 88–94; b) M. R. Whitaker, A. Parulkar, N. A. Brunelli, *Mol. Syst. Des. Eng.* **2020**, *5*, 257–268.
[12] a) M. Niakan, M. Masteri-Farahani, F. Seidi, *Fuel* **2023**, *337*, 127242; b) M. Niakan, M. Masteri-Farahani, F. Seidi, *Renew. Energy* **2023**, *212*, 50–56.
[13] J. R. Deka, D. Saikia, H.-H. G. Tsai, K.-T. Chen, W.-H. Kuan, H.-C. Hsu, H.-M. Kao, Y.-C. Yang, *ChemistrySelect* **2022**, *7*, e202202357.
[14] Z. Liu, Z. Sun, D. Qin, G. Yang, *React. Kinet. Mech. Catal.* **2019**, *128*, 523–538.
[15] a) A. J. Crisci, M. H. Tucker, M.-Y. Lee, S. G. Jang, J. A. Dumesic, S. L. Scott, *ACS Catal.* **2011**, *1*, 719–728; b) C. Bispo, K. De Oliveira Vigier, M. Sardo, N. Bion, L. Mafra, P. Ferreira, F. Jérôme, *Catal. Sci. Technol.* **2014**, *4*, 2235–2240; c) B. Karimi, H. M. Mirzaei, *RSC Adv.* **2013**, *3*, 20655–20661.
[16] a) C. M. A. Parlett, K. Wilson, A. F. Lee, *Chem. Soc. Rev.* **2013**, *42*, 3876–3893; b) J. Liang, Z. B. Liang, R. Q. Zou, Y. L. Zhao, *Adv. Mater.* **2017**, *29*, 1701139.
[17] a) Y. Wan, D. Y. Zhao, *Chem. Rev.* **2007**, *107*, 2821–2860; b) Y. H. Deng, J. Wei, Z. K. Sun, D. Y. Zhao, *Chem. Soc. Rev.* **2013**, *42*, 4054–4070.
[18] D. Y. Zhao, J. Y. Sun, Q. Z. Li, G. D. Stucky, *Chem. Mater.* **2000**, *12*, 275–279.
[19] a) K. Szczodrowski, B. Prelot, S. Lantenois, J. M. Douillard, J. Zajac, *Microporous Mesoporous Mater.* **2009**, *124*, 84–93; b) T. Asefa, M. J. MacLachlan, N. Coombs, G. A. Ozin, *Nature* **1999**, *402*, 867–871.
[20] S. G. Wainwright, C. M. A. Parlett, R. A. Blackley, W. Z. Zhou, A. F. Lee, K. Wilson, D. W. Bruce, *Microporous Mesoporous Mater.* **2013**, *172*, 112–117.
[21] a) S. Siles-Quesada, C. M. A. Parlett, A. C. Lamb, J. C. Manayil, Y. Liu, J. Mensah, H. Arandiyan, K. Wilson, A. F. Lee, *Mater. Today Chem.* **2023**, *30*, 101574; b) C. M. A. Parlett, P. Keshwalla, S. G. Wainwright, D. W. Bruce, N. S. Hondow, K. Wilson, A. F. Lee, *ACS Catal.* **2013**, *3*, 2122–2129; c) C. M. A. Parlett, M. A. Isaacs, S. K. Beaumont, L. M. Bingham, N. S. Hondow, K. Wilson, A. F. Lee, *Nat. Mater.* **2016**, *15*, 178–182.
[22] a) C. M. A. Parlett, H. Arandiyan, L. J. Durndell, M. A. Isaacs, A. T. Lopez, R. J. Wong, K. Wilson, A. F. Lee, *Microporous Mesoporous Mater.* **2022**, *329*, 111535; b) C. L. Tong, R. A. Boulos, C. Z. Yu, K. S. Iyer, C. L. Raston, *RSC Adv.* **2013**, *3*, 18767–18770.
[23] a) M. Grun, I. Lauer, K. K. Unger, *Adv. Mater.* **1997**, *9*, 254–257; b) K. Yano, Y. Fukushima, *J. Mater. Chem.* **2004**, *14*, 1579–1584; c) X. Dong, Y. Wang, H. Dan, Z. H. Hong, K. J. Song, Q. Xian, Y. Ding, *Mater. Lett.* **2017**, *204*, 97–100.
[24] a) K. Zhang, L. L. Xu, J. G. Jiang, N. Calin, K. F. Lam, S. J. Zhang, H. H. Wu, G. D. Wu, B. Albela, L. Bonneviot, P. Wu, *J. Am. Chem. Soc.* **2013**, *135*, 2427–2430; b) A. B. Chen, Y. F. Yu, H. J. Lv, Y. Zhang, T. T. Xing, Y. H. Yu, *Mater. Lett.* **2014**, *135*, 43–46.
[25] a) D. K. Shen, J. P. Yang, X. M. Li, L. Zhou, R. Y. Zhang, W. Li, L. Chen, R. Wang, F. Zhang, D. Y. Zhao, *Nano Lett.* **2014**, *14*, 923–932; b) Z. G. Teng, X. D. Su, Y. Y. Zheng, J. Sun, G. T. Chen, C. C. Tian, J. D. Wang, H. Li, Y. N. Zhao, G. M. Lu, *Chem. Mater.* **2013**, *25*, 98–105; c) J. G. Wang, Q. Xiao, H. J. Zhou, P. C. Sun, D. T. Ding, T. H. Chen, *J. Colloid Interface Sci.* **2008**, *323*, 332–337.
[26] a) L. Xiong, X. Du, B. Y. Shi, J. X. Bi, F. Kleitz, S. Z. Qiao, *J. Mater. Chem. B* **2015**, *3*, 1712–1721; b) N. Gong, X. H. Wang, Y. Zhang, Z. K. Zhao, *Mater. Chem. Phys.* **2019**, *236*, 121821.
[27] D. S. Moon, J. K. Lee, *Langmuir* **2014**, *30*, 15574–15580.
[28] a) E. O. Stejskal, J. E. Tanner, *J. Chem. Phys.* **1965**, *42*, 288–292; b) K. F. Morris, C. S. Johnson, Jr., *J. Am. Chem. Soc.* **1992**, *114*, 3139–3141; c) H. Barjat, G. A. Morris, S. Smart, A. G. Swanson, S. C. R. Williams, *J. Magn. Reson. Ser. B* **1995**, *108*, 170–172; d) C. S. Johnson, *Prog. Nucl. Magn. Reson. Spectrosc.* **1999**, *34*, 203–256.
[29] a) M. D. Mantle, D. I. Enache, E. Nowicka, S. P. Davies, J. K. Edwards, C. D'Agostino, D. P. Mascarenhas, L. Durham, M. Sankar, D. W. Knight, L. F. Gladden, S. H. Taylor, G. J. Hutchings, *J. Phys. Chem. C* **2011**, *115*, 1073–1079; b) C. D'Agostino, J. Mitchell, L. F. Gladden, M. D. Mantle, *J. Phys. Chem. C* **2012**, *116*, 8975–8982; c) T. J. Rottreau, C. M. A. Parlett, A. F. Lee, R. Evans, *J. Phys. Chem. C* **2017**, *121*, 16250–16256; d) M. A. Isaacs, N. Robinson, B. Barbero, L. J. Durndell, J. C. Manayil, C. M. A. Parlett, C. D'Agostino, K. Wilson, A. F. Lee, *J. Mater. Chem. A* **2019**, *7*, 11814–11825; e) M. A. Isaacs, C. M. A. Parlett, N. Robinson, L. J. Durndell, J. C. Manayil, S. K. Beaumont, S. Jiang, N. S. Hondow, A. C. Lamb, D. Jampaiah, M. L. Johns, K. Wilson, A. F. Lee, *Nat. Catal.* **2020**, *3*, 921–931.

[30] M. Thommes, K. Kaneko, A. V. Neimark, J. P. Olivier, F. Rodriguez-Reinoso, J. Rouquerol, K. S. W. Sing, *Pure Appl. Chem.* **2015**, *87*, 1051–1069.
[31] C. Pirez, J. M. Caderon, J. P. Dacquin, A. F. Lee, K. Wilson, *ACS Catal.* **2012**, *2*, 1607–1614.
[32] C. Pirez, A. F. Lee, J. C. Manayil, C. M. A. Parlett, K. Wilson, *Green Chem.* **2014**, *16*, 4506–4509.
[33] J. J. Senkevich, C. J. Mitchell, G. R. Yang, T. M. Lu, *Langmuir* **2002**, *18*, 1587–1594.
[34] J. Shi, Y. H. Shan, Y. Tian, Y. Wan, Y. T. Zheng, Y. Y. Feng, *RSC Adv.* **2016**, *6*, 13514–13521.
[35] K. Wilson, A. F. Lee, D. J. Macquarrie, J. H. Clark, *Appl. Catal. A Gen.* **2002**, *228*, 127–133.
[36] D. Y. Zhao, J. L. Feng, Q. S. Huo, N. Melosh, G. H. Fredrickson, B. F. Chmelka, G. D. Stucky, *Science* **1998**, *279*, 548–552.
[37] J. Horvat, B. Klaić, B. Metelko, V. Šunjić, *Tetrahedron Lett.* **1985**, *26*, 2111–2114.
[38] N. A. S. Ramli, N. A. S. Amin, *Chem. Eng. J.* **2016**, *283*, 150–159.
[39] X. Li, R. Xu, J. Yang, S. Nie, D. Liu, Y. Liu, C. Si, *Ind. Crops Prod.* **2019**, *130*, 184–197.
[40] B. A. Fachri, R. M. Abdilla, H. H. van de Bovenkamp, C. B. Rasrendra, H. J. Heeres, *ACS Sustain. Chem. Eng.* **2015**, *3*, 3024–3034.
[41] G. Di Carmine, C. Leonardi, L. Forster, M. Hu, D. Lee, C. M. A. Parlett, O. Bortolini, M. A. Isaacs, A. Massi, C. D'Agostino, *ACS Appl. Mater. Interfaces* **2023**, *15*, 24528–24540.
[42] N. Rahimi, R. Karimzadeh, *Appl. Catal. A* **2011**, *398*, 1–17.
[43] T. Bligaard, R. M. Bullock, C. T. Campbell, J. G. Chen, B. C. Gates, R. J. Gorte, C. W. Jones, W. D. Jones, J. R. Kitchin, S. L. Scott, *ACS Catal.* **2016**, *6*, 2590–2602.
[44] W. L. Dai, G. J. Wu, L. D. Li, N. J. Guan, M. Hunger, *ACS Catal.* **2013**, *3*, 588–596.
[45] A. Jerschow, N. Muller, *J. Magn. Reson.* **1997**, *125*, 372–375.
[46] M. Nilsson, *J. Magn. Reson.* **2009**, *200*, 296–302.

Manuscript received: July 31, 2023
Revised manuscript received: September 29, 2023
Accepted manuscript online: October 5, 2023
Version of record online: October 24, 2023